



Polarization spectroscopy of an excited state transition in Rubidium

NOURAH F. ALMUHAWISH,^{1,2,*}  SHUYING CHEN,¹ LUCY A. DOWNES,¹ MATTHEW J. JAMIESON,¹  ANDREW R. MACKELLAR,¹ AND KEVIN J. WEATHERILL¹ 

¹Joint Quantum Centre (Durham-Newcastle), Department of Physics, Durham University, South Road, Durham DH1 3LE, United Kingdom

²Physics Department, Faculty of Science, King Faisal University, Al-Hassa, P.O.Box 400, Hofouf 31982, Saudi Arabia

*nalmuhawish@kfu.edu.sa

Abstract: We investigate polarization spectroscopy of an excited state transition in room-temperature rubidium vapor. By applying a circularly polarized coupling beam, resonant with the $5^2S_{1/2} \rightarrow 5^2P_{3/2}$ transition, we induce anisotropy in the atomic medium that is then probed by scanning a probe beam across the $5^2P_{3/2} \rightarrow 6^2S_{1/2}$ transition. By performing polarimetry on the probe beam, a dispersive spectral feature is observed. We characterize the excited-state polarization spectrum as a function of coupling intensity for both isotopes and find that at high intensities, Autler-Townes splitting results in a sub-feature, which theoretical modelling shows is enhanced by Doppler averaging. This spectroscopic technique produces a narrow dispersive signal which is ideal for laser frequency stabilization to excited-state transitions.

Published by The Optical Society under the terms of the [Creative Commons Attribution 4.0 License](https://creativecommons.org/licenses/by/4.0/). Further distribution of this work must maintain attribution to the author(s) and the published article's title, journal citation, and DOI.

1. Introduction

Spectroscopy of excited state transitions within atomic systems is of increasing relevance across many research fields. For example, in recent years there has been an explosion of interest in highly-excited Rydberg atoms for numerous applications including; nonlinear optics [1], quantum computing [2] and simulation [3,4], RF sensing [5,6] and terahertz imaging [7,8]. High resolution spectroscopy of atomic excited states has also allowed the study of fundamental phenomena such as aggregate formation [9], Rydberg antiblockade [10] and nonequilibrium phase transitions [11,12]. Other applications of excited state spectroscopy include optical filtering [13,14], laser frequency up-conversion [15] and studies of the transfer of orbital angular momentum [16].

Previously, detailed studies have been performed of excited-state spectroscopy in caesium vapor including linewidth narrowing [17], effects due to wavelength mismatch [18] and double-resonance optical pumping polarization spectroscopy [19]. Many studies have been conducted on polarization spectroscopy in ground state transitions including [20,21]. In this paper, we perform a detailed study of polarization spectroscopy for an excited-state transition in both ^{85}Rb and ^{87}Rb and we find similar results to previous studies in Cs vapour by Carr *et al.* [22]. This technique can provide a signal with zero-crossing lineshape that is ideal for laser frequency stabilization. We generate a signal that has either positive or negative slope depending on the Rabi frequency of the coupling laser.

2. Experiment

The experimental setup used to study polarization spectroscopy of an excited state transition is shown in Fig. 1(a). A circularly polarized coupling beam at 780 nm (1.2 mm $1/e^2$ beam

radius) counter-propagates with a weak, linearly polarized probe beam at 1366 nm (1.6 mm $1/e^2$ beam radius). The beams are combined using dichroic mirrors and directed through a vapor cell containing ^{85}Rb and ^{87}Rb in natural abundance. The relevant atomic energy levels for ^{85}Rb are shown in Fig. 1(b). The coupling laser is frequency stabilized to the $5^2S_{1/2}|F=3\rangle \rightarrow 5^2P_{3/2}|F'=4\rangle$ transition using polarization spectroscopy and the frequency of the probe laser is swept across the $5^2P_{3/2}|F'=4\rangle \rightarrow 6^2S_{1/2}|F''=3\rangle$ transition. After passing through the cell, the probe beam traverses a polarizing beam splitter (PBS), oriented at 45° to the plane of polarization of the beam. The PBS splits the probe beam in two beams of orthogonal linear polarisation and directs each to a photodiode resulting in signals S_1 and S_2 . Note that when there is no birefringence in the medium we expect $S_1 = S_2$. The frequency of the probe laser is calibrated using a Fabry-Perot etalon (not shown) with free spectral range of 1 GHz. A probe beam power of $27 \mu\text{W}$ is used throughout and coupling powers of up to 5 mW are used.

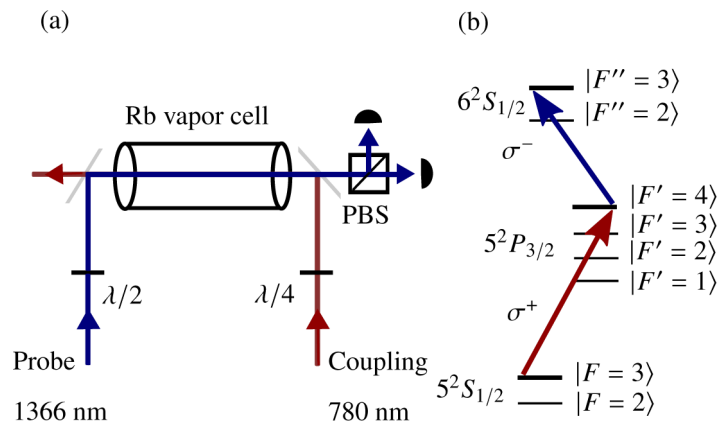


Fig. 1. (a) Experimental setup: A linearly-polarized probe beam (blue arrow) counter-propagates with a circularly polarized coupling beam (red arrow). A dichroic mirror is used to overlap the beams and direct them through a rubidium vapor cell. A polarizing beam splitter (PBS) analyzes the rotation of the probe beam that is detected after the cell using a differencing photodiode (DPD). (b) Schematic of the hyperfine structure of the atomic states in ^{85}Rb relevant to the excited-state polarization spectroscopy. The ground state, $5S_{1/2} |F=3\rangle$, is coupled to the intermediate state, $5P_{3/2} |F'=4\rangle$, by a coupling laser with wavelength $\lambda = 780 \text{ nm}$. The intermediate state is then coupled to the excited state $6S_{1/2} |F''=3\rangle$ by a probe laser with $\lambda = 1366 \text{ nm}$.

3. Result and discussion

The photodiode signals S_1 and S_2 are shown in Fig. 2(a) and (b), the transmission of the probe beam $(S_1 + S_2)/2$ which is a Lorentzian profile for ^{85}Rb is shown in Fig. 2(c). When the signals are subtracted, a dispersive lineshape results, $(S_1 - S_2)/2$ is plotted in Fig. 2(d), we call this the polarization spectrum. The measurement in Fig. 2 corresponds to coupling power of $200 \mu\text{W}$ and $27 \mu\text{W}$ probe power. The origin of the feature in the polarization spectrum can be understood as follows; assuming a quantization axis along the direction of propagation of the probe beam, the circularly polarized coupling beam induces anisotropy in the atomic medium by driving σ^+ transitions and preferentially pumping population towards states with higher m_F . On the excited state transition, the linearly polarized probe beam, which can be considered to be a superposition of left and right circular polarization is used to couple states with $|F'=4\rangle$ to $|F''=3\rangle$ and therefore the component of the probe beam which drives σ^- transitions is preferentially absorbed because there are no allowed σ^+ transitions. The difference in absorption coefficients between left and

right circularly polarized beam has a Lorentzian profile. According to the Kramers-Kronig relation [23], associated with the change in absorption coefficients is a concomitant change in the refractive index, where the difference in the refractive indices between left and right circularly polarized beam gives rise to the dispersion shaped signal. This dispersive signal provides a convenient, modulation-free signal suitable for laser frequency stabilization. A smaller feature can be observed at approximately +70 MHz, corresponding to excitation via the $|F' = 3\rangle$ state. The observed hyperfine splitting is scaled by the ratio of the wavelengths of the beams [24].

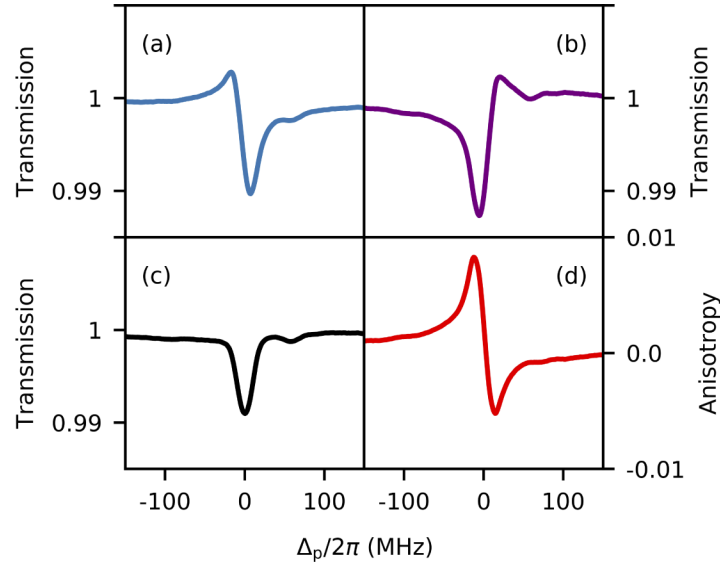


Fig. 2. (a) and (b) Probe transmission signals recorded individually from each photodiode S_1 (blue line) and S_2 (purple line), (c) the average transmission $(S_1 + S_2)/2$ of these two signals. (d) The difference of the Probe transmission signals $(S_1 - S_2)/2$ is a dispersive profile. A small peak at around +70 MHz can be observed which is due to the $F'=3$ hyperfine state.

We study the evolution of the excited state polarization spectroscopy signal as the coupling power is increased as shown in Fig. 3(a-e). As the coupling power increases we observe the dispersive signal broaden and increase in size before a second sub-Doppler dispersive signal, with opposite sign to the original feature, appears on resonance. The magnitude of this sub-feature and the linewidth of the main signal increases with increasing coupling power, as power broadening and then Autler-Townes splitting (ATS) occurs in the intermediate state as a result of saturating the ground state transition.

Polarization spectroscopy can be investigated via numerical modelling, whereby the atomic system is simplified to a coupled, three-level scheme and we use the optical Bloch equations to find the steady-state solution. The optical Bloch equations arise from solving the Lindblad master equation for the time evolution of the density matrix that is given by [25]

$$\frac{d\hat{\rho}}{dt} = -\frac{i}{\hbar}[\hat{\mathcal{H}}_{\text{tot}}, \hat{\rho}] + \hat{\mathcal{L}} \quad (1)$$

where $\hat{\mathcal{H}}_{\text{tot}}$ is the total Hamiltonian for the three-level atom-light system, $\hat{\rho}$ is the density matrix, wherein states $|1\rangle$, $|2\rangle$ and $|3\rangle$ correspond to atomic levels $5S_{1/2}$, $5P_{3/2}$ and $6S_{1/2}$ respectively. The dephasing matrix $\hat{\mathcal{L}}$ describes the decay and dephasing in the system.

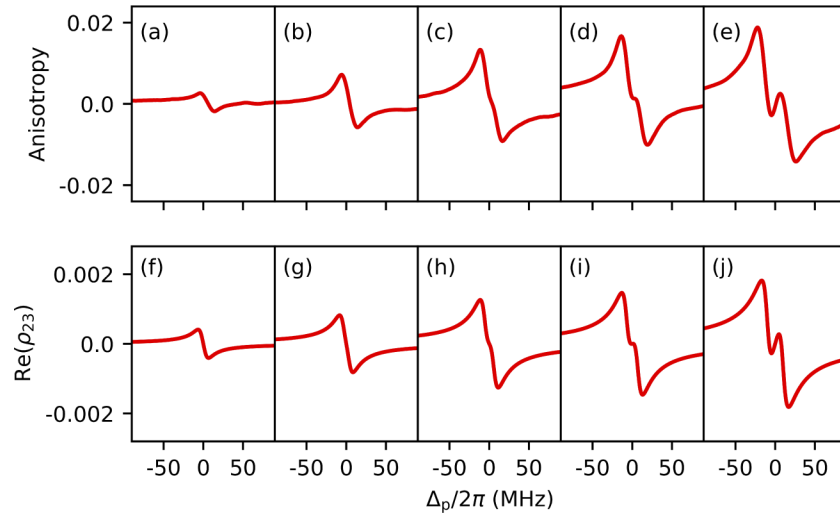


Fig. 3. (a-e) Excited-state polarisation spectroscopy signals with varying coupling power experimentally and (f-j) theoretically by solving the real part of the steady-state probe coherence in optical Bloch equations. The experiment and theory qualitatively look similar and due to Autler-Townes splitting of the intermediate state a sub-feature appears at a critical value by coupling laser Rabi frequency. Experimental parameters: Probe laser Rabi frequency $\Omega_p/2\pi = 2.7$ MHz, and coupling laser $\Omega_c/2\pi =$ (a) 6.9 MHz (50 μ W), (b) 13.9 MHz (0.2 mW), (c) 21.9 MHz (0.5 mW), (d) 27.8 MHz (0.8 mW) and (e) 43.9 MHz (2.0 mW). Theoretical parameters: Probe laser Rabi frequency $\Omega_p/2\pi = 2.7$ MHz, and coupling laser $\Omega_c/2\pi =$ (f) 2.8 MHz, (g) 4.6 MHz, (h) 7.3 MHz, (i) 9 MHz and (j) 12.7 MHz.

The total Hamiltonian of the interaction between the atom and the light for the three-level atomic system can be written as:

$$\hat{\mathcal{H}}_{\text{tot}} = \hbar \begin{pmatrix} 0 & \Omega_c/2 & 0 \\ \Omega_c/2 & -\Delta_c & \Omega_p/2 \\ 0 & \Omega_p/2 & -(\Delta_p + \Delta_c) \end{pmatrix} \quad (2)$$

where Ω_c is the coupling laser Rabi frequency between the ground state and intermediate state with detuning Δ_c and Ω_p is the probe laser Rabi frequency between the intermediate state and the excited state with detuning Δ_p .

For simplicity the decay operator $\hat{\mathcal{L}}$ is split into two separate parts; the first part describing the atomic decay, $\hat{\mathcal{L}}_{\text{atom}}$, and the second part describing the dephasing, $\hat{\mathcal{L}}_{\text{dephasing}}$, that results from the effect of the finite linewidths of the driving fields. Then, the total operator can be defined as the sum of these two parts, $\hat{\mathcal{L}} = \hat{\mathcal{L}}_{\text{atom}} + \hat{\mathcal{L}}_{\text{dephasing}}$, so the phenomenological decay matrix $\hat{\mathcal{L}}$ for a 3-level system is defined as [26]:

$$\hat{\mathcal{L}} = \begin{pmatrix} \Gamma_2 \rho_{22} & -\gamma_{12} \rho_{12} & -\gamma_{13} \rho_{13} \\ -\gamma_{12} \rho_{21} & \Gamma_3 \rho_{33} - \Gamma_2 \rho_{22} & -\gamma_{23} \rho_{23} \\ -\gamma_{13} \rho_{31} & -\gamma_{23} \rho_{32} & -\Gamma_3 \rho_{33} \end{pmatrix} \quad (3)$$

where Γ_3 is the decay rate from the excited state $|3\rangle$ to the intermediate state $|2\rangle$, Γ_2 is the decay rate from the intermediate state $|2\rangle$ to the ground state $|1\rangle$, and $\Gamma_1 = 0$ by assuming there is no decay out from the lowest level.

The decay terms can be written as:

$$\gamma_{12} = \frac{\Gamma_2}{2} + \gamma_c, \quad (4a)$$

$$\gamma_{23} = \frac{\Gamma_2 + \Gamma_3}{2} + \gamma_p, \quad (4b)$$

$$\gamma_{13} = \frac{\Gamma_3}{2} + \gamma_p + \gamma_c \quad (4c)$$

where γ_p and γ_c are the terms of the dephasing decay due to the finite linewidth of the probe and coupling field respectively.

By inserting the total Hamiltonian \hat{H}_{tot} (Eq. (2)) and the decay matrix $\hat{\mathcal{L}}$ (Eq. (3)) into Eq. (1), we can obtain the equation of motion for the density matrix element ($\dot{\rho}_{23}$):

$$\dot{\rho}_{23} = -\frac{i\Omega_p}{2}(\rho_{33} - \rho_{22}) - \frac{i\Omega_c}{2}\rho_{13} - (i\Delta_p + \gamma_{23})\rho_{23}. \quad (5)$$

Solving Eq. (5) with $\dot{\rho}_{23}=0$ and employing a perturbative technique [17] gives the solution of the steady-state probe coherence element of the density matrix (ρ_{23}):

$$\rho_{23} = \frac{\frac{i\Omega_c^2\Omega_p\gamma_{12}}{4}}{\Gamma_1\Delta_c^2 + \Gamma_1\gamma_{12}^2 + \gamma_{12}\Omega_c^2} \left[1 + \frac{\gamma_c(1 + \frac{i\Delta_c}{\gamma_{12}})}{\gamma_{23} + i\Delta_p} \right] \times \left[\gamma_{13} + i(\Delta_p + \Delta_c) + \frac{\frac{\Omega_c^2}{4}}{\gamma_{23} + i\Delta_p} \right]^{-1} \quad (6)$$

To incorporate the effect of inhomogenous Doppler broadening into our model, we can make substitutions in our total Hamiltonian (Eq. (2)) modifying the probe detuning, $\Delta_p \rightarrow \Delta_p - k_p \cdot v$ and coupling detuning, $\Delta_c \rightarrow \Delta_c + k_c \cdot v$, where $k_{p,c}$ is the wave vector of the probe/coupling light and v is the component of the atomic velocity in the direction of probe beam propagation. The optical response of the system can then be modelled by summing the contributions of each velocity class of atoms scaled in accordance with the Maxwell-Boltzmann distribution at room temperature.

Using this model, we can calculate and plot the steady state probe coherence between the intermediate and excited states, as a function of the probe detuning, parameterized by the coupling laser Rabi frequency, as shown in Fig. 3(f-j). The resulting dispersive signal provides good qualitative agreement with experimental traces.

The coupling Rabi frequency between intermediate and excited states can be expressed as

$$\Omega_c = \frac{d_{23}}{\hbar} \sqrt{\frac{4P}{c\epsilon_0\pi w^2}} \quad (7)$$

where P is the peak beam power and w is the beam waist of the coupling laser. d_{23} is the dipole moment between intermediate and excited states. The experimental Rabi frequencies parameters are systematically higher than suggested by the theory; however, in our model we have made the assumption that the dipole moment is dominated by the closed transition, $5^2P_{3/2}|m_{F'}=4\rangle \rightarrow 6^2S_{1/2}|m_{F''}=3\rangle$ which is the largest possible value. In reality, in addition to the closed transition there will be on average, a smaller effective dipole moment because the population will be distributed amongst all the m_F states and the dipole moment will be an average over these states. Furthermore, the beams have a Gaussian intensity profile which means that the Rabi frequency varies spatially across the beam, leading to inhomogenous broadening because

each atom experiences a different Rabi frequency. The effective dipole moment and the Rabi frequency variation could go some way to explaining the disparity between the experimental and modelled parameters.

In order to investigate the conditions under which ATS occurs and the sub-feature appears, we measured the on-resonance gradient of the signal for varying coupling power at two-photon resonance, i.e. at $\Delta_p = 0$ as shown in Fig. 4. It can be seen that initially, the magnitude of the on-resonance gradient increases with increasing coupling power, up to a maximum around 0.3 mW. The slope then begins to decrease as the splitting occurs, before changing sign and increasing, before levelling off at higher powers. We observe the coupling power at which the on-resonance feature changes sign to be approximately 0.8 mW. Figure 4 displays very similar trends for ^{85}Rb and ^{87}Rb .

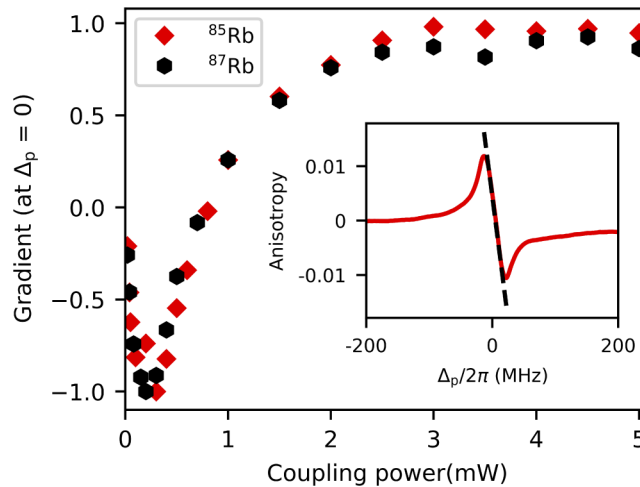


Fig. 4. On-resonance gradient, normalised to the maximum gradient of the polarisation spectroscopy signals for ^{85}Rb and ^{87}Rb when Δ_p is on resonance with varying coupling power. The inset figure is the dispersive signal from ^{85}Rb at coupling power of 0.2 mW.

To highlight how the sub-feature is dependent on Doppler averaging, we demonstrate how the different velocity classes contribute to the overall signal. Figure 5 highlights the effect of including Doppler averaging in the modelling of the sub-feature. When we probe on the excited state transition, the real part of the steady-state probe coherence between the intermediate and excited state $\text{Re}(\rho_{23})$ is equivalent to the difference in the refractive index, and that is proportional to the probe dispersion signal, shown in our experimental spectra. The dispersive signal has an on resonance gradient with negative sign if all the atoms are presumed to be at rest as seen in Fig. 5(a). By considering the contributions from varying velocity classes, shown in Fig. 5(b), the Doppler-averaged shape and the evolution of the sub-feature can be extracted by integrating over all velocity classes, resulting in the lineshape in Fig. 5(c). We modeled the atomic distribution by summing over velocity classes separated by 2 m/s with a maximum velocity of $v_{max} = 200$ m/s. We cut off the computation here because increasing the velocity does not make a difference in the shape of the signal any more. We weight the contribution to the lineshape from each velocity class by the number of atoms in that class. The simulation parameters are probe laser Rabi frequency $\Omega_p/2\pi = 3.7$ MHz, a coupling laser Rabi frequency $\Omega_c/2\pi = 12.8$ MHz and a temperature $T = 293$ K. We conclude from our model that the onset of the narrow sub-feature due to ATS is enhanced by the contributions of atoms with non-zero velocity and occurs at a lower coupling power in thermal atoms than would be the case for cold atoms. Similar phenomena of

different lineshapes and narrow sub-features generated by Doppler averaging have been observed in other pump-probe experiments [27–29].

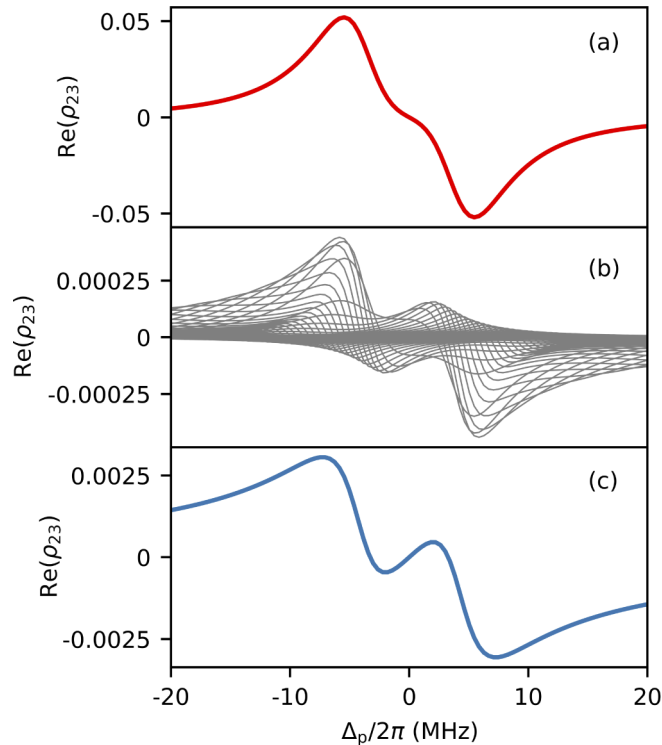


Fig. 5. The theoretical modelling of Doppler averaging on excited-state polarisation spectroscopy signal as a function of probe laser detuning Δ_p with different atomic velocity classes. The steady-state probe coherence $\text{Re}(\rho_{23})$ is proportional to the dispersion signal. (a) is the lineshape for $v = 0$. (b) non-zero velocity classes, $v_{max} = 200$ m/s and each velocity class separated by 2 m/s. (c) is the Doppler-averaged lineshape, where the contributions of non-zero velocity classes evaluate the sub-feature.

4. Conclusion

In conclusion, we have investigated excited state polarization spectroscopy in room-temperature rubidium vapor and its evolution as a function of coupling power. We characterised the onset of a dispersive sub feature and illustrated, via theoretical modelling, how this feature is enhanced by Doppler averaging. The narrow dispersion signal generated is ideal for laser frequency stabilization due to its sharp derivative and simple experimental setup. In future work we will utilize this technique for laser frequency stabilization in Rydberg atom electrometry [5] and terahertz imaging [8] experiments.

Funding. Deanship of Scientific Research, King Faisal University (216094); Engineering and Physical Sciences Research Council (EP/R002061/1, EP/S015973/1).

Acknowledgments. We acknowledge funding from UK Engineering and Physical Sciences Research Council EP/R002061/1 and EP/S015973/1. N. A. acknowledges support from the Ministry of Education in Saudi Arabia, and Saudi Arabian Cultural Bureau in London for making it possible to undertake this work. This work funded by DeanShip of scientific research (DSR), King Faisal University, Al-Hassa, KSA under Grant No. 216094. N. A. thanks the DSR for technical and financial support. We thank Ifan Hughes for useful discussions.

Disclosures. The authors declare no conflicts of interest.

Data availability. Data underlying the results presented in this paper are available in [30]

References

1. J. D. Pritchard, D. Maxwell, A. Gauguet, K. J. Weatherill, M. Jones, and C. S. Adams, "Cooperative atom-light interaction in a blockaded rydberg ensemble," *Phys. Rev. Lett.* **105**(19), 193603 (2010).
2. M. Saffman, T. G. Walker, and K. Mølmer, "Quantum information with rydberg atoms," *Rev. Mod. Phys.* **82**(3), 2313–2363 (2010).
3. A. Browaeys and T. Lahaye, "Many-body physics with individually controlled rydberg atoms," *Nat. Phys.* **16**(2), 132–142 (2020).
4. H. Bernien, S. Schwartz, A. Keesling, H. Levine, A. Omran, H. Pichler, S. Choi, A. S. Zibrov, M. Endres, M. Greiner, V. Vuletić, and M. D. Lukin, "Probing many-body dynamics on a 51-atom quantum simulator," *Nature* **551**(7682), 579–584 (2017).
5. J. A. Sedlacek, A. Schwettmann, H. Kübler, R. Löw, T. Pfau, and J. P. Shaffer, "Microwave electrometry with rydberg atoms in a vapour cell using bright atomic resonances," *Nat. Phys.* **8**(11), 819–824 (2012).
6. C. L. Holloway, J. A. Gordon, S. Jefferts, A. Schwarzkopf, D. A. Anderson, S. A. Miller, N. Thaicharoen, and G. Raithel, "Broadband rydberg atom-based electric-field probe for si-traceable, self-calibrated measurements," *IEEE Trans. Antennas Propag.* **62**(12), 6169–6182 (2014).
7. C. G. Wade, N. Šibalić, N. R. de Melo, J. M. Kondo, C. S. Adams, and K. J. Weatherill, "Real-time near-field terahertz imaging with atomic optical fluorescence," *Nat. Photonics* **11**(1), 40–43 (2017).
8. L. A. Downes, A. R. MacKellar, D. J. Whiting, C. Bourgenot, C. S. Adams, and K. J. Weatherill, "Full-field terahertz imaging at kilohertz frame rates using atomic vapor," *Phys. Rev. X* **10**(1), 011027 (2020).
9. A. Urvoy, F. Ripka, I. Lesanovsky, D. Booth, J. P. Shaffer, T. Pfau, and R. Löw, "Strongly correlated growth of rydberg aggregates in a vapor cell," *Phys. Rev. Lett.* **114**(20), 203002 (2015).
10. D. Kara, A. Bhowmick, and A. K. Mohapatra, "Rydberg interaction induced enhanced excitation in thermal atomic vapor," *Sci. Rep.* **8**(1), 5256 (2018).
11. C. Carr, R. Ritter, C. Wade, C. S. Adams, and K. J. Weatherill, "Nonequilibrium phase transition in a dilute rydberg ensemble," *Phys. Rev. Lett.* **111**(11), 113901 (2013).
12. D.-S. Ding, H. Busche, B.-S. Shi, G.-C. Guo, and C. S. Adams, "Phase diagram and self-organizing dynamics in a thermal ensemble of strongly interacting rydberg atoms," *Phys. Rev. X* **10**, 021023 (2020).
13. R. Billmers, S. Gayen, M. Squicciarini, V. Contarino, W. Scharpf, and D. Allocca, "Experimental demonstration of an excited-state faraday filter operating at 532 nm," *Opt. Lett.* **20**(1), 106–108 (1995).
14. B. Luo, L. Yin, J. Xiong, J. Chen, and H. Guo, "Induced-dichroism-excited atomic line filter at 1529 nm," *IEEE Photonics Technol. Lett.* **10**(2), 021023 (2020).
15. T. Meijer, J. White, B. Smeets, M. Jeppesen, and R. Scholten, "Blue five-level frequency-upconversion system in rubidium," *Opt. Lett.* **31**(7), 1002–1004 (2006).
16. R. F. Offer, A. Daffurn, E. Riis, P. F. Griffin, A. S. Arnold, and S. Franke-Arnold, "Gouy phase-matched angular and radial mode conversion in four-wave mixing," *Phys. Rev. A* **103**(2), L021502 (2021).
17. M. Tanasittikosol, C. Carr, C. Adams, and K. Weatherill, "Subnatural linewidths in two-photon excited-state spectroscopy," *Phys. Rev. A* **85**(3), 033830 (2012).
18. A. Urvoy, C. Carr, R. Ritter, C. S. Adams, K. J. Weatherill, and R. Löw, "Optical coherences and wavelength mismatch in ladder systems," *J. Phys. B: At., Mol. Opt. Phys.* **46**(24), 245001 (2013).
19. B. Yang, Y. Liu, and J. Wang, "Double resonance optical pumping-polarization spectroscopy of an excited state transition," *Opt. Commun.* **474**, 126102 (2020).
20. C. Wieman and T. W. Hänsch, "Doppler-free laser polarization spectroscopy," *Phys. Rev. Lett.* **36**(20), 1170–1173 (1976).
21. C. Pearman, C. Adams, S. Cox, P. Griffin, D. Smith, and I. Hughes, "Polarization spectroscopy of a closed atomic transition: applications to laser frequency locking," *J. Phys. B: At., Mol. Opt. Phys.* **35**(24), 5141–5151 (2002).
22. C. Carr, C. S. Adams, and K. J. Weatherill, "Polarization spectroscopy of an excited state transition," *Opt. Lett.* **37**(1), 118–120 (2012).
23. R. W. Boyd, *Nonlinear optics* (Academic Press, 2020).
24. A. Mohapatra, T. Jackson, and C. Adams, "Coherent optical detection of highly excited rydberg states using electromagnetically induced transparency," *Phys. Rev. Lett.* **98**(11), 113003 (2007).
25. M. Fox, *Quantum Optics: An Introduction*, vol. 15 (Oxford University, 2006).
26. J. Gea-Banacloche, Y.-q. Li, S.-z. Jin, and M. Xiao, "Electromagnetically induced transparency in ladder-type inhomogeneously broadened media: Theory and experiment," *Phys. Rev. A* **51**(1), 576–584 (1995).
27. C. Ye, A. Zibrov, Y. V. Rostovtsev, and M. Scully, "Unexpected doppler-free resonance in generalized double dark states," *Phys. Rev. A* **65**(4), 043805 (2002).
28. M. Bason, A. Mohapatra, K. Weatherill, and C. Adams, "Narrow absorptive resonances in a four-level atomic system," *J. Phys. B: At., Mol. Opt. Phys.* **42**(7), 075503 (2009).
29. D. J. Whiting, E. Bimbard, J. Keaveney, M. A. Zentile, C. S. Adams, and I. G. Hughes, "Electromagnetically induced absorption in a nondegenerate three-level ladder system," *Opt. Lett.* **40**(18), 4289–4292 (2015).
30. <http://doi.org/10.15128/r23t945q78t>.